SAND2019-14487C

Sandia National Laboratories

The unstructured APhiD: A finite element formulation of Maxwell's equations using Lorenz-gauged potentials

Chester J Weiss[1,2], Christine M Downs[3] and Bart G van Bloemen Waanders[4]

SUMMARY

Multi-physics investigations of the physiochemical state of Earth's interior typically include electromagnetic interrogation methods because of their high sensitivity to pore-scale fluids and the strong contrasts in electrical conductivity associated with contrasts in lithology and the presence of volumetrically small, but electrically conductive mineral phases on grain boundaries. Efficient methods for computing Earth's three-dimensional electromagnetic response are cornerstone to such investigations as they inform experiment design, provide a platform for computational hypothesis testing, and are the primary computational engine (and bottleneck) for three-dimensional inversion. In this presentation we report recent advances in the Cartesian A-Phi method (Weiss, Computers and Geosciences, 2013) where Lorenz-gauged potentials efficiently sparsified the linear system of equations resulting from finite volume discretization of Maxwell's equations to yield solutions over frequencies spanning 9-decades of magnitude, including dominantly diffusive, wave, and mixed propagation regimes. Here, a similar analytic framework has been cast in terms of a generalized variational problem, and more specifically, a finite element solution for unstructured discretizations. Such discretizations allow for spatially variable model resolution that was simply absent in the earlier, Cartesian implementation. We demonstrate, again, how the Lorenz-gauge leads to matrix sparsification and, ultimately, reduced computational burden when compared with the Coulomb gauge. These, and other, computational innovations will be exercised through exemplar problems derived from near-surface studies of wetland environments where the subsurface electrical contrasts are extreme and the scales in relevant model features are incompatible with Cartesian discretization.

1. Problem Setup

We are interested in developing and analyzing computationally efficient methods for solving the ultra-broadband, full frequency spectrum, Maxwell's equations for applications in subsurface interrogation and characterization. The analysis therefore applies to low-frequency, inductive methods where the effects of dielectric material properties are dominated by the Ohmic conductivity, to high-frequency radar applications where the converse holds, and to mixed diffusion/propagation problems.

Our principal simplifying assumption for this study is that magnetic permeability μ_0 is assumed constant, whereas the complex electrical conductivity $\hat{\sigma}$ is a function of frequency, ω, ohmic (linear) conductivity σ, and electric permittivity, ε.

$$\hat{\sigma} = \sigma + \mathrm{i}\omega\varepsilon$$
$$\mu = \mu_0 = 4\pi \times 10^{-7}\ \mathrm{H/m}$$

Because of the divergence-free property of magnetic induction vector, **B**, it may by expressed as the curl of a vector potential, **A**. This results, via Faraday's Law, in the electric field, **E**, being represented as the sum of the frequency-scaled vector potential and the negative gradient of the electric scalar potential Φ. Notice in the static limit (ω =0), **E** reduces to the familiar form for DC resistivity analysis.

$$\nabla \cdot \mathbf{B} = 0 \longrightarrow \mathbf{B} = \nabla \times \mathbf{A}$$
$$\mathbf{E} = -\mathrm{i}\omega\mathbf{A} - \nabla\Phi$$

Substituting these definitions for **B** = μ_0**H** and **E** into Ampere's Law with sourcing term **J**s yields the starting, "curl-curl" equation for the analysis that follows. For convenience, the squared complex wavenumber is defined accordingly as $k^2 = \mathrm{i}\omega\mu_0\hat{\sigma}$.

$$\nabla \times \mathbf{H} = \mathbf{J}_{\mathrm{tot}} = \mathbf{J}_{\mathrm{s}} + \hat{\sigma}\mathbf{E}$$
$$\nabla \times \nabla \times \mathbf{A} + \mathrm{i}\omega\mu_0\hat{\sigma}\mathbf{A} + \mu_0\hat{\sigma}\nabla\Phi = \mu_0\mathbf{J}_{\mathrm{s}}$$

2. Gauging for Uniqueness

By introducing the vector and scalar potentials above, the 3 coupled equations (for each vector component of the curl-curl equation) are insufficient to guarantee uniqueness of our, now, 4 degrees of freedom. Hence, an auxiliary condition, the gauge condition, is introduced. One choice is the Coulomb gauge: $\nabla \cdot \mathbf{A} = 0$.

In the context of *nodal* finite element analysis, this is perhaps the most popular approach (Biro and Preis, 1989, Everett and Schultz, 1996; Badea et al., 2001, Puzyrev et al., 2013) and the strategy is to add -grad(div(A)) to the curl-curl equation, which by identity simplifies to a vector Laplacian equation provided the gauge condition is met.

$$\nabla \times \nabla \times \mathbf{A} - \nabla\Big(\nabla \cdot \mathbf{A}\Big) + \mathrm{i}\omega\mu_0\hat{\sigma}\mathbf{A} + \mu_0\hat{\sigma}\nabla\Phi = \mu_0\mathbf{J}_{\mathrm{s}}$$
$$-\nabla^2\mathbf{A} + k^2\mathbf{A} + \mu_0\hat{\sigma}\nabla\Phi = \mu_0\mathbf{J}_{\mathrm{s}}$$

The gauge condition is met by re-introducing the current-continuity condition along with appropriate boundary conditions for the potentials at the limits of the analysis domain.

$$\nabla \cdot \Big(\mathrm{i}\omega\hat{\sigma}\mathbf{A} + \hat{\sigma}\nabla\Phi\Big) = \nabla \cdot \mathbf{J}_{\mathrm{s}}$$

Note that in the first equation, the gradient of the scalar potential (red box) couples all 4 unknowns together, whereas in the latter equation, it's the divergence of $^{\sigma}$**A** (red box). Except in circumstances where the potentials are constant, these coupling terms are non-zero throughout the analysis domain.

Other variants of the Coulomb gauge approach include mixed mimetic edge/nodal elements where the vector potential is projected onto the space of divergence-free Whitney elements, thereby minimizing the troublesome null space of the curl operator while simultaneously satisfying the Gauge condition by construction (Ansari and Farquharson, 2014; Ansari et al., 2017).

3. The Lorenz Gauge

An alternative choice of gauge is the Lorenz gauge (no 't'), $\nabla \cdot \mathbf{A} = -\mu_0\hat{\sigma}\Phi$, which has (at least) one attractive property, not shared by the Coulomb Gauge. Expanding the curl-curl operator in the terminal equation from Section 1, above, the vector Laplacian operator is again introduced along with the grad-div operator. Substitution of the Lorenz gauge condition eliminates the grad(div(**A**)) term, replacing it with a grad(Φ), which in turn modifies the coupling term (green box). Notice that in contrast to the case with Coulomb Gauge (Section 2), the coupling term is now restricted spatially to regions where the conductivity gradient is non-zero. In other words, for Earth models consisting of piecewise blocky conductivity sub-regions, this equation is effectively the (well behaved) vector Helmholtz equation, sourced, in part, by internal boundary conditions for each of these sub-regions.

$$-\nabla^2\mathbf{A} + k^2\mathbf{A} - \mu_0\Big(\nabla\left(\hat{\sigma}\Phi\right) - \hat{\sigma}\nabla\Phi\Big) = \mu_0\mathbf{J}_{\mathrm{s}}$$
$$= \Phi\nabla\hat{\sigma}$$

Similarly, re-introduction of the current-continuity condition and substitution of the Lorenz gauge condition therein, brings forth an elliptic equation for the electric potential, coupled as before to the vector potential through the electrical conductivity gradient (green box).

$$\nabla \cdot \Big(\mathrm{i}\omega\hat{\sigma}\mathbf{A} + \hat{\sigma}\nabla\Phi\Big) = \nabla \cdot \mathbf{J}_{\mathrm{s}}$$
$$\mathrm{i}\omega\Big(\hat{\sigma}\nabla \cdot \mathbf{A} + \mathbf{A} \cdot \nabla\hat{\sigma}\Big) + \nabla \cdot \left(\hat{\sigma}\nabla\Phi\right) = \nabla \cdot \mathbf{J}_{\mathrm{s}}$$
$$-\nabla \cdot \hat{\sigma}\nabla\Phi + \hat{\sigma}k^2\Phi + \mathrm{i}\omega\Big(\hat{\sigma}\nabla \cdot \mathbf{A} - \nabla \cdot \left(\hat{\sigma}\mathbf{A}\right)\Big)$$
$$= -\mathbf{A} \cdot \nabla\hat{\sigma}$$

4. Lorenz Gauge Coupling

To determine whether the locality of the Lorenz-gauged coupling terms is preserved in a finite element formulation, we take the usual step of casting them into weak form, with test functions denoted by a tilde and unit direction vectors by ***n, x, y*** and ***z***. Focusing on the coupling terms from the vector Helmholtz equation, with the prescription that conductivity σ_e is piecewise constant over elements Ω_e with boundaries Γ_e this term reduces to a sum of surface integrals over interior element boundaries plus the boundary condition on Γ of the domain Ω.

$$\int_\Omega \tilde{\mathbf{A}} \cdot \Big(\hat{\sigma}\nabla\Phi - \nabla\left(\hat{\sigma}\Phi\right)\Big)\,\mathrm{d}\Omega = \int_\Omega \hat{\sigma}\nabla \cdot \left(\Phi\tilde{\mathbf{A}}\right) - \nabla \cdot \left(\hat{\sigma}\Phi\tilde{\mathbf{A}}\right)\mathrm{d}\Omega$$
$$= \sum_e \hat{\sigma}_e \int_{\Gamma_e} (\boldsymbol{n} \cdot \tilde{\mathbf{A}})\Phi\,\mathrm{d}\Gamma \;-\; \int_\Gamma \hat{\sigma}(\boldsymbol{n} \cdot \tilde{\mathbf{A}})\Phi\,\mathrm{d}\Gamma$$

Expansion of element-wise surface integral terms over a given facet *e* with nodal basis functions ϕ_e shows that the sum of subsequent integrations over a given facet between adjacent elements of equal conductivity is identically zero due to the change in sign of the unit normal vector, ***n***.

$$\mathbf{A} = u\boldsymbol{x} + v\boldsymbol{y} + w\boldsymbol{z} \qquad \tilde{\mathbf{A}} = \tilde{u}\boldsymbol{x} + \tilde{v}\boldsymbol{y} + \tilde{w}\boldsymbol{z} \qquad \boldsymbol{n} = n_x\boldsymbol{x} + n_y\boldsymbol{y} + n_z\boldsymbol{z}$$

$$\int_{\Gamma_e} \hat{\sigma}_e\Big(\boldsymbol{n} \cdot \tilde{\mathbf{A}}\Big)\Phi\,\mathrm{d}\Gamma = \int_{\Gamma_e} \hat{\sigma}_e\Big(n_x\tilde{u} + n_y\tilde{v} + n_z\tilde{w}\Big)\Phi\,\mathrm{d}\Gamma$$
$$= \left(\tilde{\boldsymbol{u}}_e^T, \tilde{\boldsymbol{v}}_e^T, \tilde{\boldsymbol{w}}_e^T\right) \int_{\Gamma_e} \hat{\sigma}_e \begin{pmatrix} n_x\boldsymbol{\phi}_e\boldsymbol{\phi}^T \\ n_y\boldsymbol{\phi}_e\boldsymbol{\phi}^T \\ n_z\boldsymbol{\phi}_e\boldsymbol{\phi}^T \end{pmatrix} \boldsymbol{\Phi}_e\,\mathrm{d}\Gamma$$

A similar cancellation occurs for the coupling terms in the current-conservation equation, where we find the element-wise coupling matrix (yellow box) to simply be the transpose of the coupling matrix just derived.

$$\int_\Omega \tilde{\Phi}\Big(\hat{\sigma}\nabla \cdot \mathbf{A} - \nabla \cdot \left(\hat{\sigma}\mathbf{A}\right)\Big)\,\mathrm{d}\Omega = \int_\Omega \hat{\sigma}\nabla \cdot \left(\tilde{\Phi}\mathbf{A}\right) - \nabla \cdot \left(\hat{\sigma}\tilde{\Phi}\mathbf{A}\right)\mathrm{d}\Omega$$
$$= \sum_e \hat{\sigma}_e \int_{\Gamma_e} (\boldsymbol{n} \cdot \mathbf{A})\tilde{\Phi}\,\mathrm{d}\Gamma \;-\; \int_\Gamma \hat{\sigma}(\boldsymbol{n} \cdot \mathbf{A})\tilde{\Phi}\,\mathrm{d}\Gamma$$

$$\int_{\Gamma_e} \hat{\sigma}_e\Big(\boldsymbol{n} \cdot \mathbf{A}\Big)\tilde{\Phi}\,\mathrm{d}\Gamma = \int_{\Gamma_e} \hat{\sigma}_e\Big(n_x u + n_y v + n_z w\Big)\tilde{\Phi}\,\mathrm{d}\Gamma$$
$$= \tilde{\Phi}_e^T \int_{\Gamma_e} \hat{\sigma}_e \left(n_x\boldsymbol{\phi}_e\boldsymbol{\phi}^T, n_y\boldsymbol{\phi}_e\boldsymbol{\phi}^T, n_z\boldsymbol{\phi}_e\boldsymbol{\phi}^T\right) \begin{pmatrix} \boldsymbol{u}_e \\ \boldsymbol{v}_e \\ \boldsymbol{w}_e \end{pmatrix} \mathrm{d}\Gamma$$

5. Coulomb Gauge Coupling

$$\int_\Omega \tilde{\mathbf{A}} \cdot \Big(\hat{\sigma}\nabla\Phi\Big)\,\mathrm{d}\Omega = \int_\Omega \hat{\sigma}\nabla \cdot \left(\Phi\tilde{\mathbf{A}}\right) - \hat{\sigma}\Phi\Big(\nabla \cdot \tilde{\mathbf{A}}\Big)\,\mathrm{d}\Omega$$
$$= \sum_e \hat{\sigma}_e \int_{\Gamma_e} (\boldsymbol{n} \cdot \tilde{\mathbf{A}})\Phi\,\mathrm{d}\Gamma \;+\; \int_\Omega \hat{\sigma}\Phi(\nabla \cdot \tilde{\mathbf{A}})\,\mathrm{d}\Omega$$

$$\int_\Omega \tilde{\Phi}\hat{\sigma}\nabla \cdot \mathbf{A}\,\mathrm{d}\Omega = \int_\Omega \hat{\sigma}\nabla \cdot \left(\tilde{\Phi}\mathbf{A}\right) - \hat{\sigma}\Big(\mathbf{A} \cdot \nabla\tilde{\Phi}\Big)\,\mathrm{d}\Omega$$
$$= \sum_e \hat{\sigma}_e \int_{\Gamma_e} (\boldsymbol{n} \cdot \mathbf{A})\tilde{\Phi}\,\mathrm{d}\Gamma \;-\; \int_\Omega \hat{\sigma}\mathbf{A} \cdot \nabla\tilde{\Phi}\,\mathrm{d}\Omega$$

For completeness, the coupling terms of the Coulomb gauge are further analyzed to see determine whether they, too, can be simplified. As is the case with the Lorenz gauge, a sum of surface integrations over elements (with outward pointing normal) can be partitioned from the initial integration. And like before, subsequent integrations over neighboring elements with equal conductivity results in cancellation of these terms. However, the residual from this partitioning is yet another volume integration over the complete computational domain. Since there is no requirement that the test functions $\tilde{\mathbf{A}}$ adhere to some gauge or that $\nabla\tilde{\Phi} = 0$, these volume integrals persist in the final finite element matrix assembly, resulting in a much greater density of non-zero coupling matrix elements than one would find in the Lorenz gauged case (except in the pathological case where each element differs in conductivity from its neighbors).

6. Numerical Results

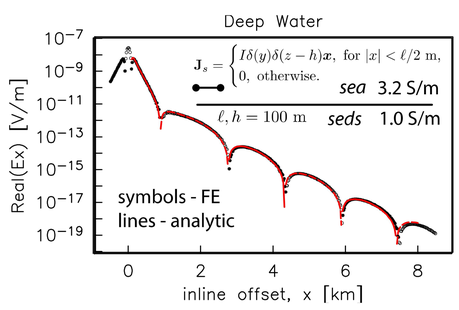

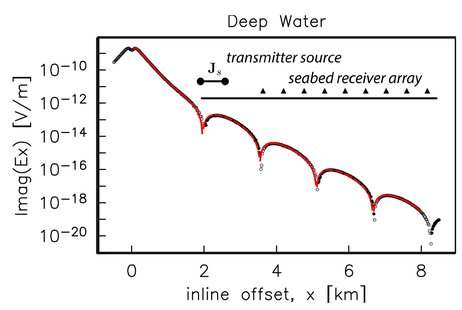

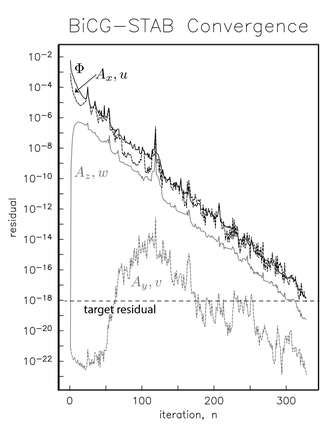

Finite element analysis was done using linear nodal basis functions, with a matrix-free variant of the iterative BiCG-STAB linear solver. Benchmarking (top) and BiCG-STAB convergence (right) for the "deep water" marine CSEM example described in Weiss (2013). Mesh is composed of 240k nodes on 1.4M tets. Tet facets on the sea/sed interface couple the sea and sed regions according to the surface integrals described above. Convergence is analyzed in terms of the Ax, Ay, Az and Phi equations of the global FE system of linear equations.

Closer to home, a near-surface example based on the EM-31 ground conductivity meter shows excellent agreement between FE and analytic solutions for both vertical and horizontal modes (above, left). In this example, a mesh with 113k nodes on 652k elements discretizes is used, where the EM-31 transmitter (TX) and receiver (RX) coils are approximated by mesh-conforming loops 0.1 m in radius. Excitation of a buried 0.1 S/m conductive lens (2 m thick and 20 m radius, located 5 m deep in a 0.001 S/m resistive background) by the EM-31 instrument (above, center and right) reveal the pattern of horizontal and vertical electric fields within the disk which give rise, in part, to the measured magnetic field in the EM-31 receiver coil.

U.S. DEPARTMENT OF ENERGY
National Nuclear Security Administration

Sandia National Laboratories is a multimission laboratory managed and operated by National Technology &Engineering Solutions of Sandia, LLC, a wholly owned subsidiary of Honeywell International Inc., for the U.S. Department of Energy's National Nuclear Security Administration under contract DE-NA0003525.
SAND No. _____

Affiliations

1. Sandia National Laboratories, Geophysics Department, cjweiss@sandia.gov
2. University of New Mexico, Earth and Planetary Sciences Dept, cjweiss@unm.edu
3. University of South Florida Libraries, cmdowns@usf.edu
4. Sandia National Laboratories, Uncertainty Quantification Department, bartv@sandia.gov

References

Ansari S and CG Farquharson, 3D finite element forward modeling of electromagnetic data using vector and scalar potentials on unstructured grids, *Geophysics*, **79**, E149-E165 (2014).

Ansari SM, CG Farquharson and SP MacLachlan, A gauged finite-element potential formulation for accurate inductive and galvanic modeling of 3-D electromagnetic problems, *Geophysical Journal International*, **210**, 105-129 (2017).

Badea EA, ME Everett, GA Newman and O Biro, Finite element analysis of controlled-source electromagnetic induction using Coulomb-gauged potentials, *Geophysics*, **66**, 786-799 (2001).

Biro O and K Preis, On the use of magnetic vector potential in in the finite element analysis of three-dimensional eddy currents, *IEEE Transactions on Magnetics*, **25**, 3145-3159 (1989).

Everett ME and A Schultz, Geomagnetic induction in a heterogeneous sphere: Azimuthally symmetric test computations and the response of and undulating 660-km discontinuity, *Journal of Geophysical Research*, **101(B2),** 2865-2783 (1996).

Puzyrev V, J Koldan, J de la Puente, G Houzeaux, M Vazquez and JM Cela, A parallel finite-element method for three-dimensional controlled-source electromagnetic forward modelling, *Geophysical Journal International*, **193**, 678-693 (2013).

Weiss CJ, Project APhiD: A Lorenz-gauged A-Phi decomposition for parallelized computation of ultra-broadband electromagnetic induction in a fully heterogeneous Earth, *Computers & Geosciences*, **58**, 40-52 (2013).

Sandia National Laboratories

THE UNIVERSITY OF NEW MEXICO